

JOURNAL OF GLACIOLOGY



CAMBRIDGE
UNIVERSITY PRESS

THIS MANUSCRIPT HAS BEEN SUBMITTED TO THE JOURNAL OF GLACIOLOGY AND HAS NOT BEEN PEER-REVIEWED.

Future projections for the Antarctic ice sheet until the year 2300 with a climate-index method

Journal:	<i>Journal of Glaciology</i>
Manuscript ID	JOG-22-0052
Manuscript Type:	Article
Date Submitted by the Author:	13-May-2022
Complete List of Authors:	Greve, Ralf; Hokkaido University, Institute of Low Temperature Science; Hokkaido University, Arctic Research Center Chambers, Christopher; Hokkaido University, Institute of Low Temperature Science Obase, Takashi; The University of Tokyo, Atmosphere and Ocean Research Institute Saito, Fuyuki; JAMSTEC, RIGC Chan, Wing-Le; The University of Tokyo, Atmosphere and Ocean Research Institute Abe-Ouchi, Ayako; The University of Tokyo, Atmosphere and Ocean Research Institute
Keywords:	Antarctic glaciology, Climate change, Ice and climate, Ice-sheet modelling
Abstract:	As part of the Coupled Model Intercomparison Project Phase 6 (CMIP6), the Ice Sheet Model Intercomparison Project for CMIP6 (ISMIP6) was devised to assess the likely sea-level-rise contribution from the Earth's

	<p>ice sheets. Here, we construct an ensemble of climate forcings for Antarctica until the year 2300 based on original ISMIP6 forcings until 2100, combined with climate indices from simulations with the MIROC4m climate model until 2300. We then use these forcings to run simulations for the Antarctic ice sheet with the SICOPOLIS model. For the unabated warming pathway RCP8.5/SSP5-8.5, the ice sheet suffers a severe mass loss, amounting to ~ 1.5 m SLE (sea-level equivalent) for the fourteen-experiment mean, and ~ 3.3 m SLE for the most sensitive experiment. Most of this loss originates from West Antarctica. For the reduced emissions pathway RCP2.6/SSP1-2.6, the loss is limited to a three-experiment mean of ~ 0.16 m SLE. The means are approximately two times larger than what was found in a previous study (Chambers and others, 2022, doi: 10.1017/jog.2021.124) that assumed a sustained late-21st-century climate beyond 2100, demonstrating the importance of continuously projected Antarctic climate change in the 22nd and 23th centuries.</p>

SCHOLARONE™
Manuscripts

Future projections for the Antarctic ice sheet until the year 2300 with a climate-index method

Ralf GREVE^{1,2}, Christopher CHAMBERS¹, Takashi OBASE³, Fuyuki SAITO⁴,
Wing-Le CHAN³, Ayako ABE-OUCHI³

¹*Institute of Low Temperature Science, Hokkaido University, Sapporo, Japan*

²*Arctic Research Center, Hokkaido University, Sapporo, Japan*

³*Atmosphere and Ocean Research Institute, University of Tokyo, Kashiwa, Japan*

⁴*Japan Agency for Marine-Earth Science and Technology, Yokohama, Japan*

Correspondence: Ralf Greve <greve@lowtem.hokudai.ac.jp>

ABSTRACT. As part of the Coupled Model Intercomparison Project Phase 6 (CMIP6), the Ice Sheet Model Intercomparison Project for CMIP6 (ISMIP6) was devised to assess the likely sea-level-rise contribution from the Earth's ice sheets. Here, we construct an ensemble of climate forcings for Antarctica until the year 2300 based on original ISMIP6 forcings until 2100, combined with climate indices from simulations with the MIROC4m climate model until 2300. We then use these forcings to run simulations for the Antarctic ice sheet with the SICOPOLIS model. For the unabated warming pathway RCP8.5/SSP5-8.5, the ice sheet suffers a severe mass loss, amounting to ~ 1.5 m SLE (sea-level equivalent) for the fourteen-experiment mean, and ~ 3.3 m SLE for the most sensitive experiment. Most of this loss originates from West Antarctica. For the reduced emissions pathway RCP2.6/SSP1-2.6, the loss is limited to a three-experiment mean of ~ 0.16 m SLE. The means are approximately two times larger than what was found in a previous study (Chambers and others, 2022, doi: 10.1017/jog.2021.124) that assumed a sustained late-21st-century climate beyond 2100, demonstrating the importance of continuously projected Antarctic climate change in the 22nd and 23th centuries.

1 INTRODUCTION

The ice sheets of Antarctica and Greenland are the largest potential contributors to future sea-level rise caused by global warming because of their enormous volumes. These amount to 57.9 ± 0.9 m SLE (sea-level equivalent) for the Antarctic ice sheet (AIS) (Morlighem and others, 2020) and 7.42 ± 0.05 m SLE for the Greenland ice sheet (GrIS) (Morlighem and others, 2017). Observations revealed that both ice sheets have been losing substantial amounts of mass since the 1990s. For the period 2012–2017, The IMBIE Team (2018) report a mass loss of 219 ± 43 Gt a⁻¹ for the AIS, most of which originates from the West Antarctic ice sheet (WAIS), and The IMBIE Team (2020) report a loss of 244 ± 28 Gt a⁻¹ for the GrIS (IMBIE: Ice sheet Mass Balance Inter-comparison Exercise). Therefore, the recent absolute losses are of similar size (likely somewhat larger for the GrIS), whereas the relative loss (compared to the total mass) is approximately 10 times smaller for the AIS compared to the GrIS. For both ice sheets, changes in the surface mass balance (SMB) as well as dynamic changes contribute to the mass loss.

A particular threat for the WAIS is that it may undergo a rapid, catastrophic disintegration through a process known as marine-ice-sheet instability (MISI) (e.g., Weertman, 1974; Mercer, 1978; Thomas and Bentley, 1978; Schoof, 2007). In contrast to the East Antarctic ice sheet (EAIS), large parts of the WAIS are grounded on a bed which is below sea level and sloping downward inland. Therefore, an initial retreat of the grounding line causes the ice sheet to be thicker at its new location, which may increase discharge and thus mass loss, so that the grounding line retreats even further in a runaway fashion. There is paleoclimatic evidence that the WAIS collapsed during past warm periods (Pollard and DeConto, 2009; Alley and others, 2015; Dutton and others, 2015; Gasson and others, 2016; Turney and others, 2020). Recent observations indicate that a new instability may already be in its initial phase (e.g., Joughin and others, 2014; Rignot and others, 2014; The IMBIE Team, 2018).

To estimate the future contribution of the AIS and GrIS to sea-level rise until the end of the 21st century, the Ice Sheet Model Intercomparison Project for CMIP6 (ISMIP6) was devised (Nowicki and others, 2016, 2020). It is part of the Coupled Model Intercomparison Project Phase 6 (CMIP6), a major international climate modelling initiative (Eyring and others, 2016) with the main goal to provide input for the recently published Sixth Assessment Report (AR6) of the Intergovernmental Panel on Climate Change (IPCC) (IPCC, 2021). For the AIS, when forced by output from CMIP5 global climate models (GCMs), a mass loss in the range of -7.8 to 30.0 cm SLE was found under the unabated warming pathway RCP8.5

56 [RCP: Representative Concentration Pathway] (Seroussi and others, 2020). The limited number of results
57 for the reduced emissions pathway RCP2.6 fall within this range, and so do the results obtained with
58 CMIP6 climate forcings (Payne and others, 2021). This rather unclear picture for the AIS is a consequence
59 of the counteracting effects of mass loss due to ocean warming and mass gain from increased snowfall. The
60 main findings for the GrIS, when forced by output from CMIP5 GCMs, were contributions of 90 ± 50 and
61 32 ± 17 mm SLE for RCP8.5 and RCP2.6, respectively (Goelzer and others, 2020). The CMIP6 GCMs tend
62 to feature a warmer atmosphere, which results in higher mass loss due to increased surface melt (Payne
63 and others, 2021).

64 The full suite of ISMIP6 experiments with both CMIP5 and CMIP6 forcings was carried out with the
65 ice-sheet model SICOPOLIS (“SImlulation COde for POLythermal Ice Sheets”, www.sicopolis.net), as doc-
66 umented in detail by Greve and others (2020a,b). Chambers and others (2022) extended the ISMIP6 sim-
67 ulations for the AIS with SICOPOLIS until the year 3000, assuming a sustained late-21st-century climate
68 beyond 2100. Compared to the uncertain response projected over the ISMIP6 period, a radically different
69 picture emerges, demonstrating that the consequences of the high-emissions scenario RCP8.5/SSP5-8.5
70 [SSP: Shared Socioeconomic Pathway] are much greater than the 100-year response in the long term even
71 if no further climate trend is applied beyond 2100. A similar study for the GrIS was conducted by Greve
72 and Chambers (2022).

73 Other studies on the response of the AIS to longer-term climate change have also been conducted.
74 Schaeffer and others (2012) and Levermann and others (2013) used statistical relationships between past
75 temperatures and global sea levels to predict future sea-level change from all sources, including the ice
76 sheets. Golledge and others (2015) used the Parallel Ice-Sheet Model (PISM) to demonstrate that at-
77 mospheric warming in excess of 1.5 to 2°C above present, triggers ice-shelf collapse and a centennial to
78 millennial-scale response by the AIS. They simulated a contribution to sea-level rise from Antarctica under
79 higher emission scenarios of 0.6 to 3 m by the year 2300. Similarly, Garbe and others (2020) found that at
80 greater than 2°C of global average warming, the WAIS is committed to long-term partial collapse. They
81 also found distinct regimes in the rates of sea-level rise per degree, with a doubling in the rate if warming
82 becomes greater than 2°C. Bulthuis and others (2019) carried out AIS projections until 3000 based on
83 spatially uniform temperature-anomaly time-series and a combination of simulations with the fast Elemen-
84 tary Thermomechanical Ice Sheet (f.ETISh) model, an emulator, probabilistic methods and uncertainty
85 quantification. They found that, irrespective of parametric uncertainty, the WAIS remains stable under

86 RCP2.6, while RCP8.5 triggers its collapse under almost all investigated cases. In the ISMIP6-endorsed
87 Antarctic BUttrressing Model Intercomparison Project (ABUMIP; Sun and others, 2020), the response of
88 the AIS to sudden and sustained loss of ice shelves was simulated by an ensemble of 15 ice-sheet models.
89 It was found that this leads to a multi-metre (1–12 m) contribution to sea-level rise over the 500-year-long
90 simulations. Lipscomb and others (2021) used the Community Ice Sheet Model (CISM) to investigate
91 the response of the AIS to ISMIP6 ocean thermal forcings only, extended to the year 2500. They found
92 long-term retreat of the WAIS and showed that the Amundsen sector exhibits threshold behaviour with
93 modest retreat or complete collapse, depending on parameter settings in the melt scheme, ocean forcing,
94 and basal friction law. Complete collapse of the WAIS occurred under some combinations of low basal
95 friction and high thermal forcing anomalies. Van Breedam and others (2020) projected the response of the
96 AIS and GrIS 10,000 years into the future with the Earth system model of intermediate complexity LOVE-
97 CLIMv1.3 (LOVECLIM: LOch–Vecode–Ecbilt–CLio–agIsm Model), including the ice-sheet model AGISM
98 (Antarctic and Greenland Ice Sheet Model), forced by the extended concentration pathways ECP2.6, 4.5,
99 6.0 and 8.5 until 2300 and zero emissions thereafter. For the AIS, they report mass losses ranging from
100 about 1.6 m SLE for the lowest forcing scenario until up to 27 m SLE for the higher-forcing scenarios.

101 In the present study, we follow an approach similar to Chambers and others (2022), extending the
102 ISMIP6-Antarctica simulations further into the future. However, we drop the assumption of a sustained
103 climate with no warming or cooling trend beyond 2100. Instead, to account for greenhouse-gas emissions
104 pathways and climate inertia after the 21st century, we construct extensions of all ISMIP6-Antarctica
105 climate forcings until 2300 by a climate-index method explained in Sect. 2. The set-up of SICOPOLIS and
106 the 18 model experiments (1 control, 14 RCP8.5/SSP5-8.5, 3 RCP2.6/SSP1-2.6) are explained in Sect. 3.
107 The results are described in Sect. 4, and a discussion and conclusion is provided in Sect. 5.

108 2 CLIMATE FORCING

109 We construct an ensemble of climate forcings for Antarctica for the period 2015–2300 by combining re-
110 sults from MIROC4m (MIROC: Model for Interdisciplinary Research On Climate) RCP8.5 and RCP4.5
111 simulations for 1995–2300 (Bakker and others, 2016) with the ensemble of ISMIP6 forcings for 2015–2100
112 (Nowicki and others, 2020; Seroussi and others, 2020; Payne and others, 2021). To do so, we derive a set
113 of atmospheric and oceanic climate indices from the MIROC4m simulations such that 1995–2014 averages
114 of the considered fields are mapped to zero and 2091–2100 averages to unity (Sect. 2.1). We then use

115 the climate indices to extrapolate the ensemble of ISMIP6 forcings to the period 2101–2300 (Sect. 2.2).
 116 Together with the original ISMIP6 forcings, this method provides smooth climate forcings for the entire
 117 period 2015–2300.

118 2.1 Climate indices

We define five atmospheric and one oceanic climate indices. For the atmosphere, the considered fields are the mean-annual surface temperature, summer (December – January – February, DJF) surface temperature, precipitation, evaporation and surface runoff. These are spatially averaged over the AIS land grid (excluding the ice shelves because they are not contained in the MIROC4m set-up), and then mapped linearly on a dimensionless scale such that

$$\begin{aligned} c_{xx}(\text{1995–2014 average}) &= 0, \\ c_{xx}(\text{2091–2100 average}) &= 1, \end{aligned} \quad (1)$$

119 where $xx \in \{\text{ST (mean-annual surface temperature), ST_DJF (DJF surface temperature), prec (precipi-}$
 120 $\text{tation), evap (evaporation), roff (runoff)}\}$. This yields the five atmospheric climate indices c_{ST} , $c_{\text{ST_DJF}}$,
 121 c_{prec} , c_{evap} and c_{roff} .

122 For the ocean, we use the average temperature south of 62.5°S and between 200 and 800 metres depth.
 123 Non-dimensionalization with the same pinning points as defined by Eq. (1) ($xx = \text{oc}$) provides the oceanic
 124 climate index c_{oc} .

Since the MIROC4m results are available for RCP8.5 and RCP4.5, the above method provides climate indices for these two pathways. However, ISMIP6 covers RCP8.5 and RCP2.6, so that we also require the climate indices for RCP2.6. To obtain these, we extrapolate the atmospheric and oceanic indices for RCP8.5 and RCP4.5, assuming linear relations between the indices and the radiative forcing of the RCP scenarios:

$$c_{xx}^{\text{RCP2.6}} = c_{xx}^{\text{RCP4.5}} - \frac{4.5 - 2.6}{8.5 - 4.5} \times (c_{xx}^{\text{RCP8.5}} - c_{xx}^{\text{RCP4.5}}). \quad (2)$$

125 The resulting climate indices are shown in Figure 1. (Note that the scaling defined by Eq. (1) implies
 126 that, e.g., a value of 1 means a stronger climate change for RCP8.5 than for RCP2.6.) For RCP8.5, the
 127 change of all six variables during the 22nd and 23rd century goes well beyond late-21st-century levels.
 128 The five atmospheric indices evolve into a certain saturation towards the end of the period, whereas the
 129 oceanic index increases steadily. This is due to the larger inertia of the ocean compared to the atmosphere.
 130 For RCP2.6, the atmospheric indices largely fall below their late-21st-century levels, indicating a partial

131 recovery of the climate change. By contrast, the oceanic index does not show such a recovery and keeps
 132 on increasing (albeit at a decreasing rate), which again results from the larger oceanic inertia.

133 2.2 Scaling of the ISMIP forcings

134 The ISMIP6 forcings for the AIS consist of anomalies for the surface temperature
 135 $[\Delta\text{ST}(x, y, t)]$ and the surface mass balance $[\Delta\text{SMB}(x, y, t)]$ relative to 1995–2014, and absolute values
 136 for the oceanic thermal forcing $[\text{TF}(x, y, z, t)]$, all for the period 2015–2100. These were derived from a
 137 systematic sampling of CMIP5 GCMs that reflects their spread in future projections (Barthel and others,
 138 2020), while CMIP6 GCMs were added on the basis of availability only (Payne and others, 2021). The at-
 139 mospheric forcings ΔST and ΔSMB enter the ice-sheet simulations directly as upper boundary conditions.
 140 By contrast, TF is used to compute sub-ice-shelf melt rates via a non-local quadratic parameterization
 141 (“ISMIP6 standard approach”) calibrated by observations (Jourdain and others, 2020).

To extend the ISMIP6 forcings until 2300, the oceanic thermal forcing is converted to an anomaly as well:

$$\Delta\text{TF}(x, y, z, t) = \text{TF}(x, y, z, t) - \text{TF}_{1995-2014}(x, y, z), \quad t \leq 2100 \text{ CE}. \quad (3)$$

We then scale the anomalies as follows:

$$\begin{aligned} \Delta\text{ST}(x, y, t) &= c_{\text{ST}}(t) \times \Delta\text{ST}_{2091-2100}(x, y), \\ \Delta\text{prec}(x, y, t) &= c_{\text{prec}}(t) \times \Delta\text{prec}_{2091-2100}(x, y), \\ \Delta\text{evap}(x, y, t) &= c_{\text{evap}}(t) \times \Delta\text{evap}_{2091-2100}(x, y), \quad t > 2100 \text{ CE}, \\ \Delta\text{roff}(x, y, t) &= c_{\text{roff}}(t) \times \Delta\text{roff}_{2091-2100}(x, y), \\ \Delta\text{TF}(x, y, z, t) &= c_{\text{oc}}(t) \times \Delta\text{TF}_{2091-2100}(x, y, z), \end{aligned} \quad (4)$$

where Δprec , Δevap and Δroff are the anomalies of precipitation, evaporation and runoff, respectively.

The anomaly ΔSMB results from

$$\Delta\text{SMB}(x, y, t) = \Delta\text{prec}(x, y, t) - \Delta\text{evap}(x, y, t) - \Delta\text{roff}(x, y, t), \quad t > 2100 \text{ CE}, \quad (5)$$

and ΔTF is converted back to absolute values:

$$\text{TF}(x, y, z, t) = \text{TF}_{1995-2014}(x, y, z) + \Delta\text{TF}(x, y, z, t), \quad t > 2100 \text{ CE}. \quad (6)$$

142 Thus, this method provides extended ISMIP6 forcings for the AIS [$\Delta\text{ST}(x, y, t)$,
143 $\Delta\text{SMB}(x, y, t)$, $\text{TF}(x, y, z, t)$] until the year 2300.

For one of the ISMIP6 simulations, an additional ice-shelf-collapse forcing is employed. It stipulates that ice-shelf collapse occurs when the mean surface melting over the past decade exceeds a threshold value of 725 mm water equiv. a^{-1} (Trusel and others, 2015; Seroussi and others, 2020). Hereby, the mean surface melting is parameterized by an exponential function of the DJF near-surface air temperature, ST_DJF . For $t \leq 2100$ CE, ST_DJF is taken from bias-adjusted, GCM-forced simulations with the regional climate model RACMO2 (Trusel and others, 2015). For $t > 2100$ CE, we construct ST_DJF via its anomaly, $\Delta\text{ST_DJF}$, as follows:

$$\begin{aligned} \Delta\text{ST_DJF}(x, y, t) &= c_{\text{ST_DJF}}(t) \times \Delta\text{ST}_{2091-2100}(x, y), \\ \text{ST_DJF}(x, y, t) &= \text{ST}_{1995-2014}(x, y) \\ &\quad + [\text{ST_DJF}_{\text{param}}(x, y) - \text{ST}_{\text{param}}(x, y)] \\ &\quad + \Delta\text{ST_DJF}(x, y, t), \end{aligned} \quad t > 2100 \text{ CE}. \quad (7)$$

144 Note that $\Delta\text{ST}_{2091-2100}$ and $\text{ST}_{1995-2014}$ are mean-annual rather than DJF values because only these are
145 available in the ISMIP6 forcing. To convert to DJF, we use the parameterized difference [$\text{ST_DJF}_{\text{param}} -$
146 ST_{param}] of present-day DJF and mean-annual temperatures, respectively, by Fortuin and Oerlemans (1990)
147 (see also Greve and others, 2020a, their Eqs. (10) and (11)).

148 This method provides annual ice-shelf-collapse masks for the years 2101–2300. To guarantee a smooth
149 transition to the pre-2100 masks provided by ISMIP6, we define a 10-year interval 2101–2110, during which
150 the final masks are computed as weighted averages between the original ISMIP6 masks and our extended
151 ones.

152 3 MODEL EXPERIMENTS

153 We apply the ice-sheet model SICOPOLIS (Greve and SICOPOLIS Developer Team, 2022) to the AIS with
154 hybrid shallow-ice–shelvy-stream dynamics (Bernales and others, 2017) for grounded ice, shallow-shelf dy-
155 namics for floating ice, a Weertman-Budd-type sliding law tuned separately for 18 different regions (Greve
156 and others, 2020a), and ice thermodynamics treated by the one-layer melting-CTS enthalpy scheme (CTS:
157 cold-temperate transition surface; Blatter and Greve, 2015; Greve and Blatter, 2016). The horizontal reso-

158 lution is 8 km, which, in combination with the sliding law that features a continuous basal drag across the
159 grounding line, is sufficient to produced good results for the grounding line migration in both advance and
160 retreat scenarios (Gladstone and others, 2017; Chambers and others, 2022). In the vertical, we use terrain-
161 following coordinates (sigma transformation) with 81 layers in the ice domain and 41 layers in the thermal
162 lithosphere layer below. For details on the set-up, the initialization procedure by a paleoclimatic spin-up,
163 comparisons between the simulated and observed ice thickness and surface velocity for our initialization
164 year 1990, as well as the historical run (“hist”) that bridges the gap between 1990 and the start date of
165 the projections in January 2015 by employing NorESM1-M/RCP8.5 surface mass balance (SMB), surface
166 temperature (ST) and oceanic thermal forcing (TF), we refer to Greve and others (2020a). From the last
167 20 years of the historical run, we extract the 1995–2014 climatology (SMB, ST) required as a reference for
168 the future climate experiments.

169 An overview of our extended ISMIP6 experiments is given in Table 1. The method of extending the
170 ISMIP6 climate forcing until 2300 is described above (Sect. 2). 14 experiments are for the 21st-century
171 unabated warming pathway RCP8.5 (CMIP5) / SSP5-8.5 (CMIP6), and three are for the reduced emissions
172 pathway RCP2.6 (CMIP5) / SSP1-2.6 (CMIP6) that is largely in line with the commitments of the Paris
173 Agreement (maintaining the global mean temperature well below a 2°C increase above pre-industrial levels).
174 In two of the RCP8.5 experiments, the impact of different calibrations of the parameterization for sub-ice-
175 shelf melting (“high” and “low” vs. the normal, “medium” calibration, thereby exploring the uncertainty
176 of the parameterization) is tested, and one experiment employs a calibration in which only observed basal-
177 melt values near the grounding line of the Pine Island ice shelf are used (“PIGL-medium”) (Jourdain and
178 others, 2020). As already mentioned in Sect. 2.2, in one experiment, ice-shelf fracture triggered by surface
179 melting is accounted for. In addition, a projection control simulation (“ctrl_proj”) employs constant
180 climate conditions based on the 1995–2014 reference climatology.

181 4 RESULTS

182 The simulated mass change of the AIS, expressed as a sea-level contribution, is shown in Figure 2. For
183 the control run ctrl_proj, the ice sheet remains stable, showing only a minimal mass loss of 3.49 mm SLE
184 during the 286 years model time. This stability also holds for the longer control run over a 986-years period
185 until the year 3000 reported by Chambers and others (2022).

186 Until 2100, the future projections are equivalent to the original ISMIP6-Antarctica simulations carried

187 out with SICOPOLIS (Seroussi and others, 2020; Greve and others, 2020a; Payne and others, 2021),
188 characterized by a range of uncertainties from a notable mass loss to a slight mass gain and no clear
189 separation between RCP8.5/SSP5-8.5 (mean \pm 1-sigma range: 32.6 ± 67.2 mm SLE) and RCP2.6/SSP1-2.6
190 (8.4 ± 15.9 mm SLE). [Note: The values for RCP8.5/SSP5-8.5 differ from those given by Greve and others
191 (2020a) because that study excluded Exp. 13 (NorESM1-M/RCP8.5 with “PIGL-medium” calibration) for
192 the computation, which we have included here.] However, a different picture emerges in the longer term.
193 By 2300, the ice sheet ends up losing mass for all cases, and it responds much more strongly to the ensemble
194 of RCP8.5/SSP5-8.5 simulations than to the RCP2.6/SSP1-2.6 simulations. The final mass loss amounts
195 to 1.54 ± 0.84 m SLE for RCP8.5/SSP5-8.5, while it is limited to 0.164 ± 0.049 m SLE for RCP2.6/SSP1-2.6.
196 The mean values for both pathways are approximately twice as large as those found by Chambers and
197 others (2022) for a sustained late-21st-century climate (no further warming trend) beyond 2100 (Fig. 2b).

198 The influence of the ice mass loss due to oceanic forcing is explored by Exps. 5, 9, 10 (NorESM1-
199 M/RCP8.5 with “medium”, “high” and “low” calibration, respectively). The results are shown by the olive
200 lines and olive-shaded regions in Figure 2. By 2300, the simulated mass loss is $1.43^{+0.31}_{-0.20}$ m SLE. Thus,
201 the uncertainty due to these three calibrations is significant, but smaller than the uncertainty due to the
202 GCM forcings. A more extreme test is Exp. 13, which is NorESM1-M/RCP8.5 with the “PIGL-medium”
203 calibration described above. Until the mid-22nd century, this leads to an, on average, ~ 2 times larger total
204 ice-shelf basal melting than for Exp. 5 (later on, the difference becomes smaller due to ice-shelf decay). It
205 has a pronounced effect on the mass loss of the ice sheet: By 2300, it is 2.97 m SLE compared to the initial
206 1990 state, more than doubling that of Exp.5. This highlights the great sensitivity of the AIS to oceanic
207 forcing.

208 Exps. 8 and 12 (CCSM4/RCP8.5) investigate the influence of ice-shelf hydrofracture as described above
209 (included in Exp. 12). Exp. 8 is actually one of the cases that produce a mass gain of the ice sheet during
210 the 21st century. Adding ice-shelf hydrofracture via the time-dependent collapse mask in Exp. 12 reverts
211 this behaviour to a mass loss. By 2300, both experiments produce a loss, which is 1.27 m SLE for Exp. 8,
212 but 2.00 m SLE for Exp. 12. Thus, the process can act as a significant amplifier of the mass loss of the AIS.

213 In Figure 3, the sea-level contributions by 2300 are shown separately for the regions of the EAIS, the
214 WAIS and the Antarctic Peninsula (AP). Averaged across all the high-emission cases (panel a), the WAIS
215 contributes 1.28 m SLE, compared with just 0.24 m SLE from the EAIS and 0.019 m SLE from the AP. This
216 contrasts with the low-emission cases (panel b) which have average SLE contributions from the WAIS

217 and EAIS of 0.064 and 0.097 m, respectively, with the AP contribution being very slightly negative at
218 -0.00078 m. These findings agree with those by Chambers and others (2022) (simulations until 3000, no
219 further warming or cooling trend beyond 2100), and the reason for the predominant contribution from the
220 WAIS for RCP8.5/SSP5-8.5 is that it undergoes a MISI in the areas of the Amundsen Sea Embayment and
221 the Siple Coast where the bedrock bathymetry deepens inward. By contrast, the weaker climatic forcings
222 of RCP2.6/SSP1-2.6 do not trigger the WAIS instability in our simulations.

223 We now discuss in more detail the results of Exp. 6 (MIROC-ESM-CHEM/RCP8.5), which was already
224 focused on in the previous study by Chambers and others (2022). It features high atmospheric changes and
225 median ocean warming compared to the other CMIP5 GCMs (Barthel and others, 2020), and it produces
226 a $\sim 29\%$ above average mass loss of 1.99 m SLE (WAIS 1.69 m, EAIS 0.16 m, AP 0.13 m) for our combined
227 CMIP5/CMIP6 ensemble. Figure 4 shows the components of the global mass balance (integrated over the
228 ice sheet, all counted as positive for mass gain): surface mass balance (SMB), basal mass balance (BMB),
229 calving and ice volume change (dV/dt). The residual, $\text{Res} = |\text{SMB} + \text{BMB} + \text{Calving} - dV/dt|$, has a mean
230 value of $2.14 \times 10^4 \text{ m}^3 \text{ a}^{-1}$ over the 286 years simulation time. This is eight orders of magnitude smaller
231 than the typical range of values in the figure [$\mathcal{O}(10^{12} \text{ m}^3 \text{ a}^{-1})$], so that the model conserves mass very well
232 (see also Calov and others, 2018).

233 The ice sheet keeps losing volume (\propto mass) over the entire period and at an accelerating rate of change.
234 The SMB, driven by the counteracting effects of increasing precipitation and increasing runoff, remains
235 positive throughout the model time. The BMB, predominantly produced by sub-ice-shelf melting, strongly
236 increases in magnitude over time, which is the main reason for the accelerated volume loss of the ice sheet.
237 The essentially monotonic increase (except for short-term fluctuations) of the BMB contrasts with the
238 study by Chambers and others (2022) where it peaks around 2100, but then falls back to values around
239 $-4 \times 10^{12} \text{ m}^3 \text{ a}^{-1}$ between 2150 and 2300. Calving into the surrounding ocean is also a significant component
240 of the mass balance. However, it changes only moderately over time, except for a period of increased calving
241 with a peak around 2170 due to a major retreat event of the Ross Ice Shelf. The inter-annual variability
242 of the volume change is mainly due to that of the SMB and the BMB, which reflects the variability of the
243 atmospheric and oceanic forcings.

244 In Appendix A, we present a similar analysis of the global mass balance for the pair of Exps. 5 and 7
245 (NorESM1-M/RCP8.5, NorESM1-M/RCP2.6).

246 Snapshots of the simulated ice thickness and surface velocity for Exp. 6 are shown in Figure 5. By 2095,

247 the ice sheet has overall undergone only minor changes compared to the initial year 2015, corresponding to a
248 mass loss of 0.0070 m SLE. By 2195, which is just after the calving event mentioned above, the changes are
249 more notable (mass loss 0.40 m SLE). A large part of the present-day Ross Ice Shelf has disappeared, and
250 the grounding lines in the areas of the Pine Island and Thwaites glaciers and the Siple Coast have migrated
251 inland, along with a speed-up of the ice streams. A similar, yet less pronounced grounding line retreat
252 and speed-up has occurred in the area of Totten Glacier, and the northern part of the Amery Ice Shelf has
253 disintegrated. By the end of 2300 (mass loss 1.99 m SLE), the instability of the WAIS is progressing in full
254 force, with dramatic retreats of the Pine Island/Thwaites and Siple Coast grounding lines, accompanied by
255 additional retreats of the grounding line of the Filchner–Ronne Ice Shelf. In the EAIS, the Amery Ice Shelf
256 has disappeared almost entirely, and the area of Totten Glacier shows some more grounding line retreat;
257 however, with limited impact on the ice sheet further inland.

258 5 DISCUSSION AND CONCLUSION

259 The future climate simulations for the AIS until the year 2300 carried out in the present study reveal a
260 different picture compared to the original ISMIP6–Antarctica simulations for the 21st century (Seroussi
261 and others, 2020; Greve and others, 2020a; Payne and others, 2021). The latter produced a range of mass
262 changes from a small gain (due to precipitation increases) to a moderate loss, and no clear distinction
263 between the unabated warming (RCP8.5/SSP5-8.5) and reduced emissions pathways (RCP2.6/SSP1-2.6).
264 By contrast, in our extended simulations, by 2300 mass gains of the AIS do not occur any more, and the
265 mass loss under RCP8.5/SSP5-8.5 is substantially larger than that under RCP2.6/SSP1-2.6 (mean values
266 of ~ 1.5 m SLE vs. only ~ 0.16 m SLE). Most of the mass loss under RCP8.5/SSP5-8.5 originates from the
267 WAIS, which suffers a MISI in almost all simulations.

268 Compared to the previous study by Chambers and others (2022) in which a sustained late-21st-century
269 climate beyond 2100 was assumed, the response of the AIS to our extrapolated climate-change scenarios
270 is about two times larger by 2300 for both pathways. For RCP8.5/SSP5-8.5, this stronger response is
271 immediately to be expected because, as detailed in Sect. 2.1, all climate indices are well above unity
272 during the 22nd and 23rd century, which means that climate change becomes ever more serious. For
273 RCP2.6/SSP1-2.6, the situation is different because the atmospheric climate recovers to below late-21st-
274 century levels, while only the the oceanic climate index stays above unity after 2100. Evidently, the impact
275 of the increasing oceanic forcing outweighs that of the recovering atmospheric forcing, so that mass loss

276 due to sub-ice-shelf melt and subsequently enhanced drainage of grounded ice is the dominant process.

277 The threat of a WAIS instability under future climate change has already been expressed by a number
278 of previous studies (see Sect. 1 for more details). A particular feature of the ISMIP6-Antarctica set-up for
279 SICOPOLIS is that it applies an SMB correction to keep the ice sheet stable and close to observed conditions
280 in the recent past (Greve and others, 2020a). This SMB correction has significant additional accumulation
281 in the area of the Pine Island and Thwaites glaciers to prevent them from becoming unstable even before
282 the end of the spin-up simulations. It is possible that this procedure over-stabilizes the area, so that the
283 onset of the instability originating from there could be delayed. On the other hand, SICOPOLIS is quite
284 sensitive to sub-ice-shelf melting compared to other ice-sheet models (Edwards and others, 2021). This
285 factor facilitates the development of a MISI because it makes the ice sheet more sensitive to grounding-line
286 migration.

287 As already discussed by Chambers and others (2022), a weakness of the ISMIP6-type simulations is
288 the lacking feedback of the changing geometry of the ice sheet on the atmospheric forcing. While the
289 ocean thermal forcing, TF, is three-dimensional and thus changes as the ice shelves become thicker or
290 thinner, the atmospheric forcing fields, ΔST and ΔSMB , are 2D fields that were derived by GCMs under
291 the assumption of a static, present-day ice sheet. Therefore, they do not change as the ice-surface elevation
292 rises or falls. A possible improvement, also beneficial for the resolution of the forcing fields, is to reprocess
293 the GCM output by a regional climate model and compute vertical gradients of ST and SMB, so that at
294 least a linearized feedback can be implemented (Franco and others, 2012). Such a method was employed
295 for the ISMIP6-Greenland simulations and derived work (Goelzer and others, 2020; Nowicki and others,
296 2020; Greve and Chambers, 2022). Short of very demanding and computationally expensive fully coupled
297 climate–ice-sheet simulations, a further possibility is to involve snapshots of climate-model results combined
298 with more refined parameterizations for the climatic forcing, similar to the approach by Abe-Ouchi and
299 others (2013) for the paleoglaciation of the Northern Hemisphere.

300 Furthermore, future work in the direction of long-term simulations of ice-sheet response to climate
301 change should aim at employing more direct, rather than extrapolated, GCM projections beyond 2100
302 and involving an ensemble of ice-sheet models to allow an improved assessment of uncertainties. Within
303 ISMIP6, this is currently planned within a new initiative “ISMIP6-Projections2300-Antarctica” for the AIS
304 (tinyurl.com/ismip6-ais-2300, last access: 2022-05-11). In detail, this initiative focuses on projections ex-
305 tended until 2300 (as in the present study) based on CMIP5 and CMIP6 GCM outputs. Some experiments

306 will use repeated climate forcing from the late 21st century, sampled randomly between 2100 and 2300
307 (similar to the approach by Chambers and others, 2022), while others will be based on output from GCMs
308 directly run until 2300 under CMIP forcing pathways. We are planning to contribute to these projections
309 with the SICOPOLIS model.

310 **CODE AND DATA AVAILABILITY**

311 SICOPOLIS is free and open-source software, available through a persistent Git repository hosted by the
312 Alfred Wegener Institute for Polar and Marine Research (AWI) in Bremerhaven, Germany (Greve and
313 SICOPOLIS Developer Team, 2022). Detailed instructions for obtaining and compiling the code are at
314 <http://www.sicopolis.net> (last access: 2022-05-11). The output data produced for this study are available
315 at Zenodo, <https://doi.org/10.5281/zenodo.xxxxxxxx>.

316 **AUTHOR CONTRIBUTIONS**

317 Ralf Greve, Christopher Chambers and Ayako Abe-Ouchi designed the study. Takashi Obase, Fuyuki Saito,
318 Wing-Le Chan and Ayako Abe-Ouchi ran the MIROC simulations. Ralf Greve, Christopher Chambers and
319 Takashi Obase computed the climate indices and the extrapolated ISMIP6 climate forcing. Ralf Greve
320 ran the SICOPOLIS simulations with support from Christopher Chambers. All authors discussed and
321 interpreted the results. Ralf Greve wrote the manuscript with contributions from all authors.

322 **ACKNOWLEDGEMENTS**

323 We thank Jorge Bernales (MARUM Bremen) and Reinhard Calov (PIK Potsdam) for their recent
324 contributions to the development of the SICOPOLIS model. Some colour schemes of our figures were taken
325 from Paul Tol's (SRON Netherlands Institute for Space Research) online resource at
326 <https://personal.sron.nl/~pault> (last access: 2022-05-11). We thank the Climate and Cryosphere (CliC)
327 effort, which provided support for ISMIP6 through sponsoring of workshops, hosting the ISMIP6 web-
328 site and wiki, and promoting ISMIP6. We acknowledge the World Climate Research Programme, which,
329 through its Working Group on Coupled Modelling, coordinated and promoted CMIP5 and CMIP6. We
330 thank the climate modelling groups for producing their model output and making it available; the Earth
331 System Grid Federation (ESGF) for archiving the CMIP data and providing access to it; the University at

332 Buffalo for ISMIP6 data distribution and upload; and the multiple funding agencies who support CMIP5,
333 CMIP6, and ESGF. We thank the ISMIP6 steering committee, the ISMIP6 model selection group and
334 ISMIP6 dataset preparation group for their continuous engagement in defining ISMIP6. This is ISMIP6
335 contribution No. xxx.

336 *Financial support.* Ralf Greve, Christopher Chambers, Wing-Le Chan and Ayako Abe-Ouchi were
337 supported by Japan Society for the Promotion of Science (JSPS) KAKENHI Grant No. JP17H06323. Ralf
338 Greve, Wing-Le Chan and Ayako Abe-Ouchi were supported by JSPS KAKENHI Grant No. JP17H06104.
339 Takashi Obase, Fuyuki Saito and Ayako Abe-Ouchi were supported by JSPS Grant-in-Aid for Japan–France
340 Integrated Action Program (SAKURA Program) No. JPJSBP120213203.

341 REFERENCES

- 342 Abe-Ouchi A, Saito F, Kawamura K, Raymo ME, Okuno J, Takahashi K and Blatter H (2013) Insolation-driven
343 100,000-year glacial cycles and hysteresis of ice-sheet volume. *Nature*, **500**(7461), 190–193 (doi: 10.1038/nature12374)
344
- 345 Alley RB, Anandakrishnan S, Christianson K, Horgan HJ, Muto A, Parizek BR, Pollard D and Walker RT (2015)
346 Oceanic forcing of ice-sheet retreat: West Antarctica and more. *Annual Review of Earth and Planetary Sciences*,
347 **43**(1), 207–231 (doi: 10.1146/annurev-earth-060614-105344)
- 348 Bakker P, Schmittner A, Lenaerts JTM, Abe-Ouchi A, Bi D, van den Broeke MR, Chan WL, Hu A, Beadling RL,
349 Marsland SJ, Mernild SH, Saenko OA, Swingedouw D, Sullivan A and Yin J (2016) Fate of the Atlantic Meridional
350 Overturning Circulation: Strong decline under continued warming and Greenland melting. *Geophysical Research*
351 *Letters*, **43**, 12252–12260 (doi: 10.1002/2016GL070457)
- 352 Barthel A, Agosta C, Little CM, Hattermann T, Jourdain NC, Goelzer H, Nowicki S, Seroussi H, Straneo F and
353 Bracegirdle TJ (2020) CMIP5 model selection for ISMIP6 ice sheet model forcing: Greenland and Antarctica. *The*
354 *Cryosphere*, **14**(3), 855–879 (doi: 10.5194/tc-14-855-2020)
- 355 Bernales J, Rogozhina I, Greve R and Thomas M (2017) Comparison of hybrid schemes for the combination of
356 shallow approximations in numerical simulations of the Antarctic Ice Sheet. *The Cryosphere*, **11**(1), 247–265 (doi:
357 10.5194/tc-11-247-2017)
- 358 Blatter H and Greve R (2015) Comparison and verification of enthalpy schemes for polythermal glaciers and ice
359 sheets with a one-dimensional model. *Polar Science*, **9**(2), 196–207 (doi: 10.1016/j.polar.2015.04.001)

- 360 Bulthuis K, Arnst M, Sun S and Pattyn F (2019) Uncertainty quantification of the multi-centennial response of the
361 Antarctic ice sheet to climate change. *The Cryosphere*, **13**(4), 1349–1380 (doi: 10.5194/tc-13-1349-2019)
- 362 Calov R, Beyer S, Greve R, Beckmann J, Willeit M, Kleiner T, Rückamp M, Humbert A and Ganopolski A (2018)
363 Simulation of the future sea level contribution of Greenland with a new glacial system model. *The Cryosphere*,
364 **12**(10), 3097–3121 (doi: 10.5194/tc-12-3097-2018)
- 365 Chambers C, Greve R, Obase T, Saito F and Abe-Ouchi A (2022) Mass loss of the Antarctic ice sheet un-
366 til the year 3000 under a sustained late-21st-century climate. *Journal of Glaciology*, **68**(269), 605–617 (doi:
367 10.1017/jog.2021.124)
- 368 Dutton A, Carlson AE, Long AJ, Milne GA, Clark PU, DeConto R, Horton BP, Rahmstorf S and Raymo ME
369 (2015) Sea-level rise due to polar ice-sheet mass loss during past warm periods. *Science*, **349**(6244), aaa4019 (doi:
370 10.1126/science.aaa4019)
- 371 Edwards TL, Nowicki S, Marzeion B, Hock R, Goelzer H, Seroussi H, Jourdain NC, Slater DA, Turner FE, Smith CJ,
372 McKenna CM, Simon E, Abe-Ouchi A, Gregory JM, Larour E, Lipscomb WH, Payne AJ, Shepherd A, Agosta C,
373 Alexander P, Albrecht T, Anderson B, Asay-Davis X, Aschwanden A, Barthel A, Bliss A, Calov R, Chambers C,
374 Champollion N, Choi Y, Cullather R, Cuzzzone J, Dumas C, Felikson D, Fettweis X, Fujita K, Galton-Fenzi BK,
375 Gladstone R, Golledge NR, Greve R, Hattermann T, Hoffman MJ, Humbert A, Huss M, Huybrechts P, Immerzeel
376 W, Kleiner T, Kraaijenbrink P, Le clec'h S, Lee V, Leguy GR, Little CM, Lowry DP, Malles JH, Martin DF,
377 Maussion F, Morlighem M, O'Neill JF, Nias I, Pattyn F, Pelle T, Price SF, Quiquet A, Radić V, Reese R, Rounce
378 DR, Rückamp M, Sakai A, Shafer C, Schlegel NJ, Shannon S, Smith RS, Straneo F, Sun S, Tarasov L, Trusel LD,
379 Van Breedam J, van de Wal R, van den Broeke M, Winkelmann R, Zekollari H, Zhao C, Zhang T and Zwinger
380 T (2021) Projected land ice contributions to twenty-first-century sea level rise. *Nature*, **593**(7857), 74–82 (doi:
381 10.1038/s41586-021-03302-y)
- 382 Eyering V, Bony S, Meehl GA, Senior CA, Stevens B, Stouffer RJ and Taylor KE (2016) Overview of the Coupled Model
383 Intercomparison Project Phase 6 (CMIP6) experimental design and organization. *Geoscientific Model Development*,
384 **9**(5), 1937–1958 (doi: 10.5194/gmd-9-1937-2016)
- 385 Fortuin JPF and Oerlemans J (1990) Parameterization of the annual surface temperature and mass balance of
386 Antarctica. *Annals of Glaciology*, **14**, 78–84 (doi: 10.3189/S0260305500008302)
- 387 Franco B, Fettweis X, Lang C and Erpicum M (2012) Impact of spatial resolution on the modelling of the Greenland
388 ice sheet surface mass balance between 1990–2010, using the regional climate model MAR. *The Cryosphere*, **6**(3),
389 695–711 (doi: 10.5194/tc-6-695-2012)

- 390 Garbe J, Albrecht T, Levermann A, Donges JF and Winkelmann R (2020) The hysteresis of the Antarctic Ice Sheet.
391 *Nature*, **585**(7826), 538–544 (doi: 10.1038/s41586-020-2727-5)
- 392 Gasson E, DeConto RM, Pollard D and Levy RH (2016) Dynamic Antarctic ice sheet during the early to mid-Miocene.
393 *Proceedings of the National Academy of Sciences*, **113**(13), 3459–3464 (doi: 10.1073/pnas.1516130113)
- 394 Gladstone RM, Warner RC, Galton-Fenzi BK, Gagliardini O, Zwinger T and Greve R (2017) Marine ice sheet
395 model performance depends on basal sliding physics and sub-shelf melting. *The Cryosphere*, **11**(1), 319–329 (doi:
396 10.5194/tc-11-319-2017)
- 397 Goelzer H, Nowicki S, Payne A, Larour E, Seroussi H, Lipscomb WH, Gregory J, Abe-Ouchi A, Shepherd A, Simon E,
398 Agosta C, Alexander P, Aschwanden A, Barthel A, Calov R, Chambers C, Choi Y, Cuzzone J, Dumas C, Edwards
399 T, Felikson D, Fettweis X, Golledge NR, Greve R, Humbert A, Huybrechts P, Lecocq S, Lee V, Leguy G, Little
400 C, Lowry DP, Morlighem M, Nias I, Quiquet A, Rückamp M, Schlegel NJ, Slater D, Smith R, Straneo F, Tarasov
401 L, van de Wal R and van den Broeke M (2020) The future sea-level contribution of the Greenland ice sheet: a
402 multi-model ensemble study of ISMIP6. *The Cryosphere*, **14**(9), 3071–3096 (doi: 10.5194/tc-14-3071-2020)
- 403 Golledge NR, Kowalewski DE, Naish TR, Levy RH, Fogwill CJ and Gasson EGW (2015) The multi-millennial
404 Antarctic commitment to future sea-level rise. *Nature*, **526**(7573), 421–425 (doi: 10.1038/nature15706)
- 405 Greve R and Blatter H (2016) Comparison of thermodynamics solvers in the polythermal ice sheet model SICOPOLIS.
406 *Polar Science*, **10**(1), 11–23 (doi: 10.1016/j.polar.2015.12.004)
- 407 Greve R and Chambers C (2022) Mass loss of the Greenland ice sheet until the year 3000 under a sustained late-
408 21st-century climate. *Journal of Glaciology*, **68**(269), 618–624 (doi: 10.1017/jog.2022.9)
- 409 Greve R and SICOPOLIS Developer Team (2022) SICOPOLIS. GitLab, Alfred Wegener Institute for Polar and
410 Marine Research, Bremerhaven, Germany, URL <https://gitlab.awi.de/sicopolis/sicopolis>
- 411 Greve R, Calov R, Obase T, Saito F, Tsutaki S and Abe-Ouchi A (2020a) ISMIP6 future projections for the Antarctic
412 ice sheet with the model SICOPOLIS. Technical report, Zenodo (doi: 10.5281/zenodo.3971232)
- 413 Greve R, Chambers C and Calov R (2020b) ISMIP6 future projections for the Greenland ice sheet with the model
414 SICOPOLIS. Technical report, Zenodo (doi: 10.5281/zenodo.3971251)
- 415 IPCC (2021) *Climate Change 2021: The Physical Science Basis. Contribution of Working Group I to the Sixth*
416 *Assessment Report of the Intergovernmental Panel on Climate Change*. Cambridge University Press, in press
- 417 Joughin I, Smith BE and Medley B (2014) Marine ice sheet collapse potentially under way for the Thwaites Glacier
418 Basin, West Antarctica. *Science*, **344**(6185), 735–738 (doi: 10.1126/science.1249055)

- 419 Jourdain NC, Asay-Davis X, Hattermann T, Straneo F, Seroussi H, Little CM and Nowicki S (2020) A protocol for
420 calculating basal melt rates in the ISMIP6 Antarctic ice sheet projections. *The Cryosphere*, **14**(9), 3111–3134 (doi:
421 10.5194/tc-14-3111-2020)
- 422 Levermann A, Clark PU, Marzeion B, Milne GA, Pollard D, Radic V and Robinson A (2013) The multimillennial
423 sea-level commitment of global warming. *Proceedings of the National Academy of Sciences*, **110**(34), 13745–13750
424 (doi: 10.1073/pnas.1219414110)
- 425 Lipscomb WH, Leguy GR, Jourdain NC, Asay-Davis X, Seroussi H and Nowicki S (2021) ISMIP6-based projections of
426 ocean-forced Antarctic Ice Sheet evolution using the Community Ice Sheet Model. *The Cryosphere*, **15**(2), 633–661
427 (doi: 10.5194/tc-15-633-2021)
- 428 Mercer JH (1978) West Antarctic ice sheet and CO₂ greenhouse effect: a threat of disaster. *Nature*, **271**(5643),
429 321–325 (doi: 10.1038/271321a0)
- 430 Morlighem M, Williams CN, Rignot E, An L, Arndt JE, Bamber JL, Catania G, Chauché N, Dowdeswell JA, Dorschel
431 B, Fenty I, Hogan K, Howat I, Hubbard A, Jakobsson M, Jordan TM, Kjeldsen KK, Millan R, Mayer L, Mouginot
432 J, Noël BPY, O’Cofaigh C, Palmer S, Rysgaard S, Seroussi H, Siegert MJ, Slabon P, Straneo F, van den Broeke
433 MR, Weinrebe W, Wood M and Zinglensen KB (2017) BedMachine v3: Complete bed topography and ocean
434 bathymetry mapping of Greenland from multibeam echo sounding combined with mass conservation. *Geophysical
435 Research Letters*, **44**(21), 11051–11061 (doi: 10.1002/2017GL074954)
- 436 Morlighem M, Rignot E, Binder T, Blankenship D, Drews G, Rand Eagles, Eisen O, Ferraccioli F, Forsberg R, Fretwell
437 P, Goel V, Greenbaum JS, Gudmundsson H, Guo J, Helm V, Hofstede C, Howat I, Humbert A, Jokat W, Karlsson
438 NB, Lee WS, Matsuoka K, Millan R, Mouginot J, Paden J, Pattyn F, Roberts J, Rosier S, Ruppel A, Seroussi H,
439 Smith EC, Steinhage D, Sun B, van den Broeke MR, van Ommen TD, van Wessem M and Young DA (2020) Deep
440 glacial troughs and stabilizing ridges unveiled beneath the margins of the Antarctic ice sheet. *Nature Geoscience*,
441 **13**(2), 132–137 (doi: 10.1038/s41561-019-0510-8)
- 442 Nowicki S, Goelzer H, Seroussi H, Payne AJ, Lipscomb WH, Abe-Ouchi A, Agosta C, Alexander P, Asay-Davis
443 XS, Barthel A, Bracegirdle TJ, Cullather R, Felikson D, Fettweis X, Gregory JM, Hattermann T, Jourdain NC,
444 Kuipers Munneke P, Larour E, Little CM, Morlighem M, Nias I, Shepherd A, Simon E, Slater D, Smith RS, Straneo
445 F, Trusel LD, van den Broeke MR and van de Wal R (2020) Experimental protocol for sea level projections from
446 ISMIP6 stand-alone ice sheet models. *The Cryosphere*, **14**(7), 2331–2368 (doi: 10.5194/tc-14-2331-2020)
- 447 Nowicki SMJ, Payne A, Larour E, Seroussi H, Goelzer H, Lipscomb W, Gregory J, Abe-Ouchi A and Shepherd A
448 (2016) Ice Sheet Model Intercomparison Project (ISMIP6) contribution to CMIP6. *Geoscientific Model Develop-
449 ment*, **9**(12), 4521–4545 (doi: 10.5194/gmd-9-4521-2016)

- 450 Payne AJ, Nowicki S, Abe-Ouchi A, Agosta C, Alexander P, Albrecht T, Asay-Davis X, Aschwanden A, Barthel
451 A, Bracegirdle TJ, Calov R, Chambers C, Choi Y, Cullather R, Cuzzone J, Dumas C, Edwards TL, Felikson
452 D, Fettweis X, Galton-Fenzi BK, Goelzer H, Gladstone R, Golledge NR, Gregory JM, Greve R, Hattermann T,
453 Hoffman MJ, Humbert A, Huybrechts P, Jourdain NC, Kleiner T, Kuipers Munneke P, Larour E, Le clec'h S, Lee
454 V, Leguy G, Lipscomb WH, Little CM, Lowry DP, Morlighem M, Nias I, Pattyn F, Pelle T, Price SF, Quiquet
455 A, Reese R, Rückamp M, Schlegel NJ, Seroussi H, Shepherd A, Simon E, Slater D, Smith RS, Straneo F, Sun
456 S, Tarasov L, Trusel LD, Van Breedam J, van de Wal R, van den Broeke M, Winkelmann R, Zhao C, Zhang T
457 and Zwinger T (2021) Future sea level change under Coupled Model Intercomparison Project Phase 5 and Phase
458 6 scenarios from the Greenland and Antarctic ice sheets. *Geophysical Research Letters*, **48**(16), e2020GL091741
459 (doi: 10.1029/2020GL091741)
- 460 Pollard D and DeConto RM (2009) Modelling West Antarctic ice sheet growth and collapse through the past five
461 million years. *Nature*, **458**(7236), 329–332 (doi: 10.1038/nature07809)
- 462 Rignot E, Mouginot J, Morlighem M, Seroussi H and Scheuchl B (2014) Widespread, rapid grounding line retreat
463 of Pine Island, Thwaites, Smith, and Kohler glaciers, West Antarctica, from 1992 to 2011. *Geophysical Research*
464 *Letters*, **41**(10), 3502–3509 (doi: 10.1002/2014GL060140)
- 465 Schaeffer M, Hare W, Rahmstorf S and Vermeer M (2012) Long-term sea-level rise implied by 1.5°C and 2°C warming
466 levels. *Nature Climate Change*, **2**(12), 867–870 (doi: 10.1038/nclimate1584)
- 467 Schoof C (2007) Ice sheet grounding line dynamics: Steady states, stability, and hysteresis. *Journal of Geophysical*
468 *Research: Earth Surface*, **112**(F3), F03S28 (doi: 10.1029/2006JF000664)
- 469 Seroussi H, Nowicki S, Payne AJ, Goelzer H, Lipscomb WH, Abe-Ouchi A, Agosta C, Albrecht T, Asay-Davis X,
470 Barthel A, Calov R, Cullather R, Dumas C, Galton-Fenzi BK, Gladstone R, Golledge N, Gregory JM, Greve R,
471 Hatterman T, Hoffman MJ, Humbert A, Huybrechts P, Jourdain NC, Kleiner T, Larour E, Leguy GR, Lowry DP,
472 Little CM, Morlighem M, Pattyn F, Pelle T, Price SF, Quiquet A, Reese R, Schlegel NJ, Shepherd A, Simon E,
473 Smith RS, Straneo F, Sun S, Trusel LD, Van Breedam J, van de Wal RSW, Winkelmann R, Zhao C, Zhang T and
474 Zwinger T (2020) ISMIP6 Antarctica: a multi-model ensemble of the Antarctic ice sheet evolution over the 21st
475 century. *The Cryosphere*, **14**(9), 3033–3070 (doi: 10.5194/tc-14-3033-2020)
- 476 Sun S, Pattyn F, Simon EG, Albrecht T, Cornford S, Calov R, Dumas C, Gillet-Chaulet F, Goelzer H, Golledge NR,
477 Greve R, Hoffman MJ, Humbert A, Kazmierczak E, Kleiner T, Leguy GR, Lipscomb WH, Martin D, Morlighem
478 M, Nowicki S, Pollard D, Price S, Quiquet A, Seroussi H, Schlemm T, Sutter J, van de Wal RSW, Winkelmann R
479 and Zhang T (2020) Antarctic ice sheet response to sudden and sustained ice-shelf collapse (ABUMIP). *Journal*
480 *of Glaciology*, **66**(260), 891–904 (doi: 10.1017/jog.2020.67)

- 481 The IMBIE Team (2018) Mass balance of the Antarctic Ice Sheet from 1992 to 2017. *Nature*, **558**(7709), 219–222
482 (doi: 10.1038/s41586-018-0179-y)
- 483 The IMBIE Team (2020) Mass balance of the Greenland Ice Sheet from 1992 to 2018. *Nature*, **579**(7798), 233–239
484 (doi: 10.1038/s41586-019-1855-2)
- 485 Thomas RH and Bentley CR (1978) A model for Holocene retreat of the West Antarctic ice sheet. *Quaternary*
486 *Research*, **10**(2), 150–170 (doi: 10.1016/0033-5894(78)90098-4)
- 487 Trusel LD, Frey KE, Das SB, Karnauskas KB, Kuipers Munneke P, van Meijgaard E and van den Broeke MR
488 (2015) Divergent trajectories of Antarctic surface melt under two twenty-first-century climate scenarios. *Nature*
489 *Geoscience*, **8**(12), 927–932 (doi: 10.1038/ngeo2563)
- 490 Turney CSM, Fogwill CJ, Golledge NR, McKay NP, van Sebille E, Jones RT, Etheridge D, Rubino M, Thornton DP,
491 Davies SM, Ramsey CB, Thomas ZA, Bird MI, Munksgaard NC, Kohno M, Woodward J, Winter K, Weyrich LS,
492 Rootes CM, Millman H, Albert PG, Rivera A, van Ommen T, Curran M, Moy A, Rahmstorf S, Kawamura K,
493 Hillenbrand CD, Weber ME, Manning CJ, Young J and Cooper A (2020) Early Last Interglacial ocean warming
494 drove substantial ice mass loss from Antarctica. *Proceedings of the National Academy of Sciences*, **117**(8), 3996–
495 4006 (doi: 10.1073/pnas.1902469117)
- 496 Van Breedam J, Goelzer H and Huybrechts P (2020) Semi-equilibrated global sea-level change projections for the
497 next 10 000 years. *Earth System Dynamics*, **11**(4), 953–976 (doi: 10.5194/esd-11-953-2020)
- 498 Weertman J (1974) Stability of the junction of an ice sheet and an ice shelf. *Journal of Glaciology*, **13**(67), 3–11 (doi:
499 10.3189/S0022143000023327)

#	exp_id	Scenario	GCM	Ocean forcing	Ice-shelf fracture	
0	ctrl_proj	Control	—	—	—	
5	exp05	RCP8.5	NorESM1-M	Medium	No	Core experiments (Tier 1)
6	exp06	RCP8.5	MIROC-ESM-CHEM	Medium	No	
7	exp07	RCP2.6	NorESM1-M	Medium	No	
8	exp08	RCP8.5	CCSM4	Medium	No	
9	exp09	RCP8.5	NorESM1-M	High	No	
10	exp10	RCP8.5	NorESM1-M	Low	No	
12	exp12	RCP8.5	CCSM4	Medium	Yes	
13	exp13	RCP8.5	NorESM1-M	PIGL-Medium	No	
A5	expA05	RCP8.5	HadGEM2-ES	Medium	No	Extended ensemble (Tier 2)
A6	expA06	RCP8.5	CSIRO-Mk3.6.0	Medium	No	
A7	expA07	RCP8.5	IPSL-CM5A-MR	Medium	No	
A8	expA08	RCP2.6	IPSL-CM5A-MR	Medium	No	
B6	expB06	SSP5-8.5	CNRM-CM6-1	Medium	No	CMIP6 extension (Tier 2)
B7	expB07	SSP1-2.6	CNRM-CM6-1	Medium	No	
B8	expB08	SSP5-8.5	UKESM1-0-LL	Medium	No	
B9	expB09	SSP5-8.5	CESM2	Medium	No	
B10	expB10	SSP5-8.5	CNRM-ESM2-1	Medium	No	

Table 1. Extended ISMIP6-Antarctica Tier-1 and 2 future climate experiments for the period 2015–2300 discussed in this study. See Nowicki and others (2020) for references for the GCMs.

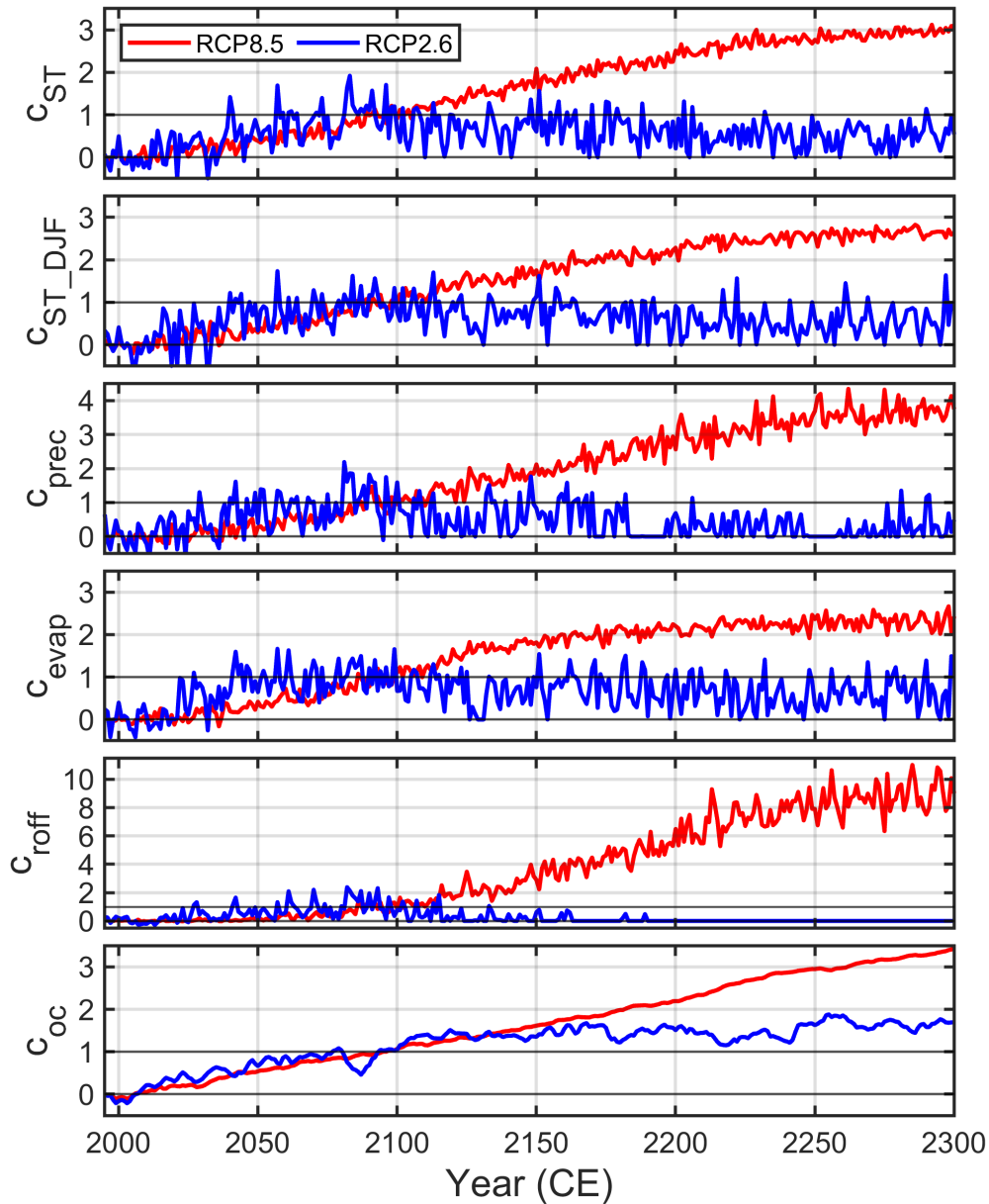


Fig. 1. RCP8.5 and RCP2.6 climate indices for the mean-annual surface temperature (c_{ST}), DJF surface temperature (c_{ST_DJF}), precipitation (c_{prec}), evaporation (c_{evap}), surface runoff (c_{roff}) and ocean temperature (c_{oc}), derived from MIROC4m simulations until the year 2300 (Bakker and others, 2016).

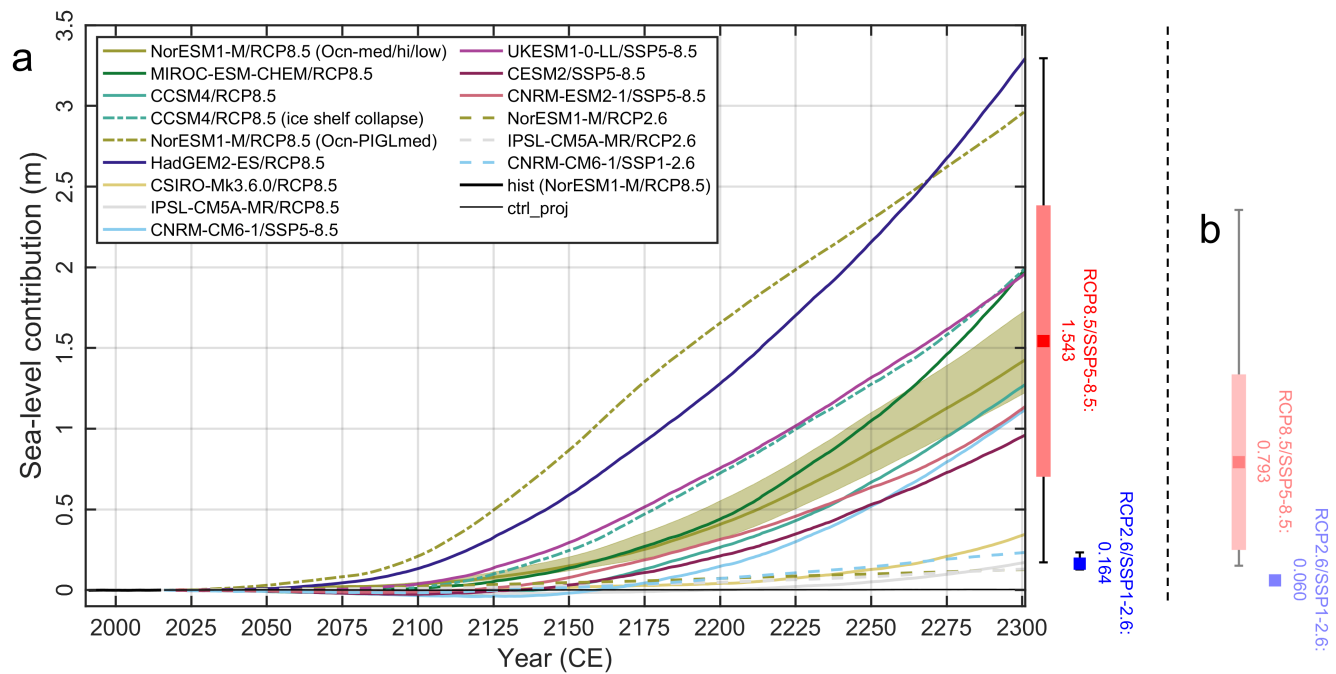


Fig. 2. (a) ISMIP6-Antarctica historical run (hist), projection control run (ctrl_proj) and Tier-1 and 2 future climate experiments extended until 2300: Simulated ice mass change, counted positively for loss and expressed as a sea-level contribution. The red and blue boxes to the right show the 2300 means for RCP8.5/SSP5-8.5 and RCP2.6/SSP1-2.6, respectively (RCP8.5/SSP5-8.5: also ± 1 -sigma); the whiskers show the corresponding full ranges. (b) Same 2300 statistics, but for the results by Chambers and others (2022) without a further warming trend beyond 2100.

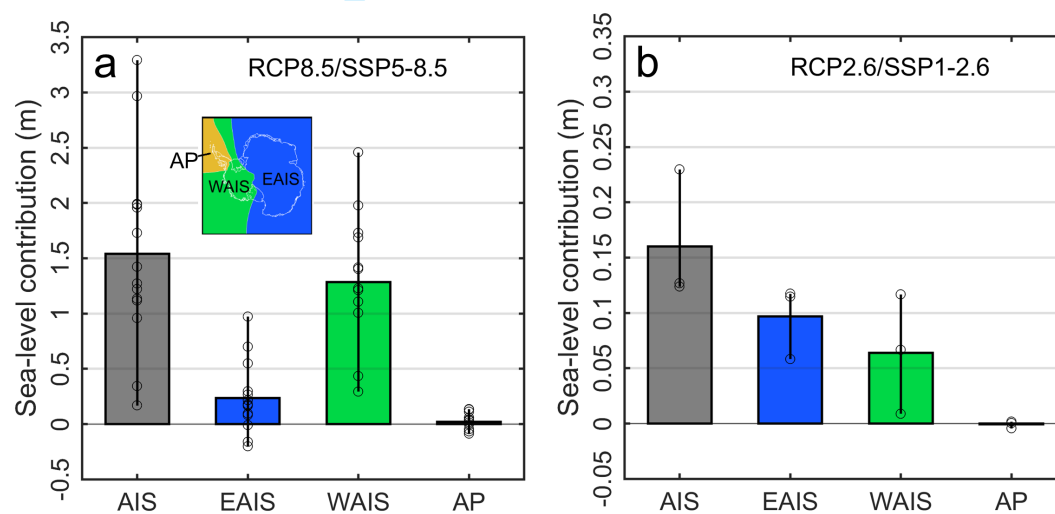


Fig. 3. Simulated sea-level contribution for the entire ice sheet and three regions (EAIS, WAIS, AP; shown in the inset) by the year 2300 relative to ctrl_proj, for (a) the RCP8.5/SSP5-8.5 and (b) the RCP2.6/SSP1-2.6 ensemble. The whiskers show the full range of sea-level contributions across the simulations that make up the means.

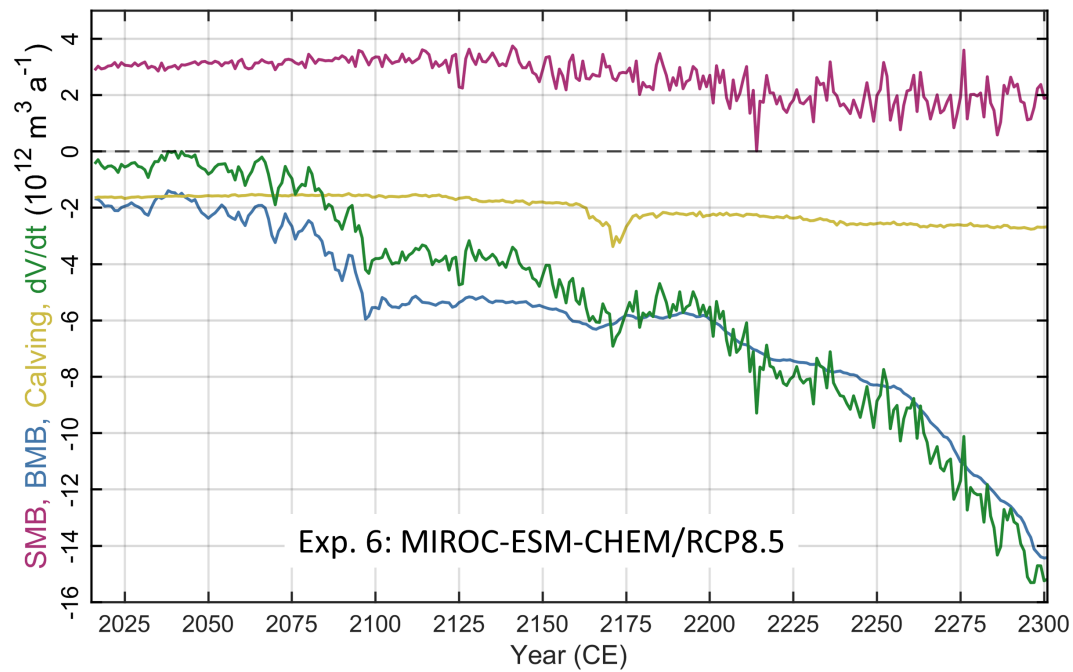


Fig. 4. Main components of the global mass balance for Exp. 6 (MIROC-ESM-CHEM/RCP8.5): Surface mass balance (SMB, purple), basal mass balance (BMB, blue), calving (yellow) and ice volume change (dV/dt , green).

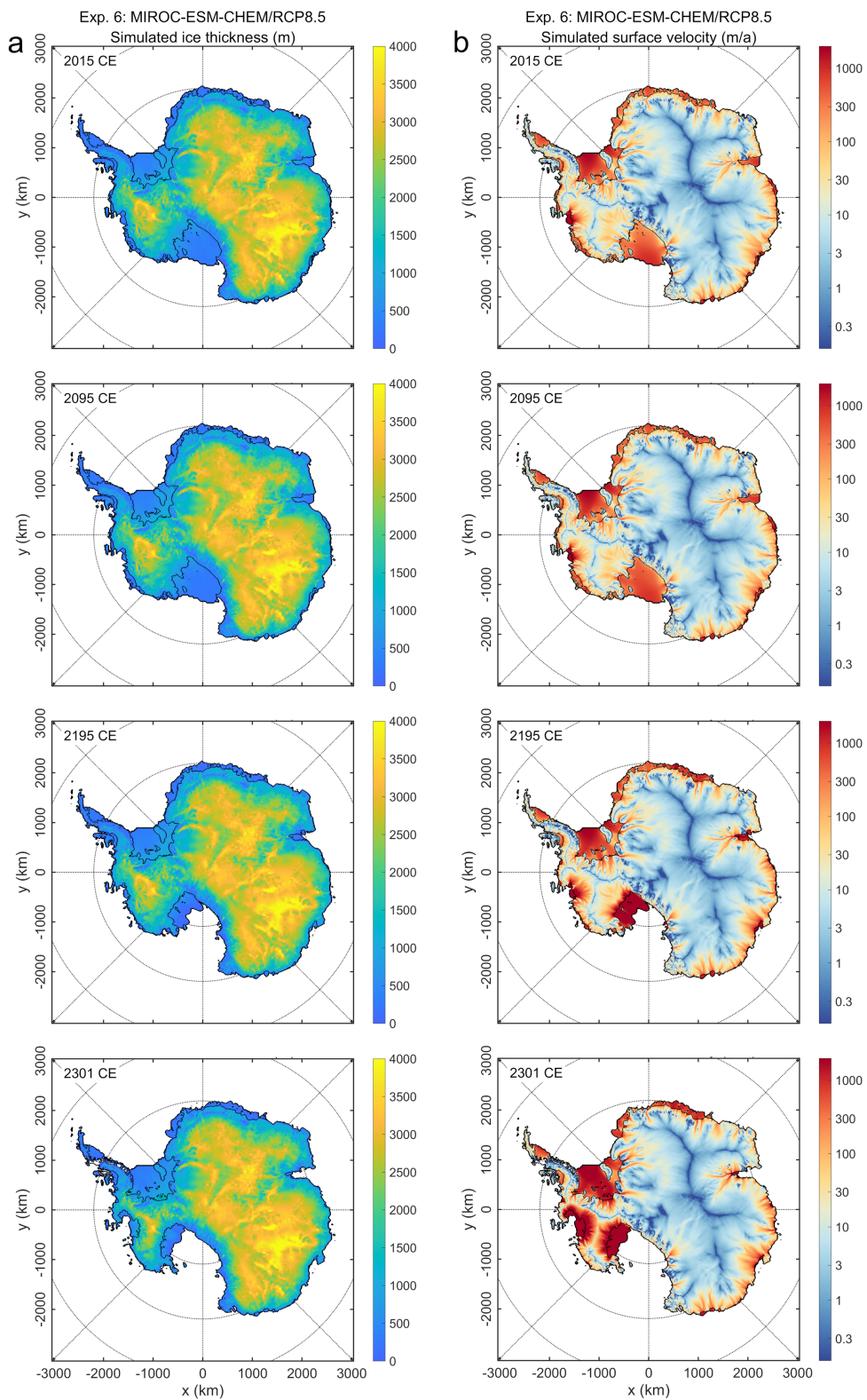


Fig. 5. Snapshots of (a) the simulated ice thickness and (b) the surface velocity for Exp. 6 (MIROC-ESM-CHEM/RCP8.5) for the years 2015, 2095, 2195 and 2301 (= end of 2300). Spacing of the latitude circles is 10° , spacing of the longitude rays is 45° .

500 A ADDITIONAL GLOBAL MASS BALANCE ANALYSIS

501 In addition to the discussion of the global mass balance for Exp. 6 (MIROC-ESM-CHEM/RCP8.5) pre-
502 sented in Sect. 4, we carry out a similar analysis for Exps. 5 and 7 (NorESM1-M/RCP8.5, NorESM1-
503 M/RCP2.6) to allow a direct comparison between an RCP8.5 and an RCP2.6 experiment (Fig. 6). By
504 the end of 2300, Exp. 5 produces a mass loss of 1.43 m SLE, lower than that of Exp. 6 and slightly below
505 the RCP8.5/SSP5-8.5 ensemble mean. The components of the global mass balance evolve generally in a
506 similar way as for Exp. 6 (Fig. 4). The most notable difference is that SMB keeps on increasing over the
507 entire model time. Further, both BMB and calving become less negative. All these factors work in the
508 same direction and contribute to the smaller mass loss.

509 The mass loss produced by Exp. 7 by the end of 2300 is 0.127 m SLE. This is the smallest value of our
510 three RCP2.6/SSP1-2.6 experiments (but almost equal to that of Exp. A8). In contrast to Exp. 5 where
511 BMB dominates, BMB and calving contribute approximately the same to the mass loss until the end of
512 the simulation. SMB is positive and almost constant. The residual between the mass gain from SMB and
513 the losses from BMB and calving is negative, but small, which leads to a net mass loss less than 10% than
514 that of Exp. 5.

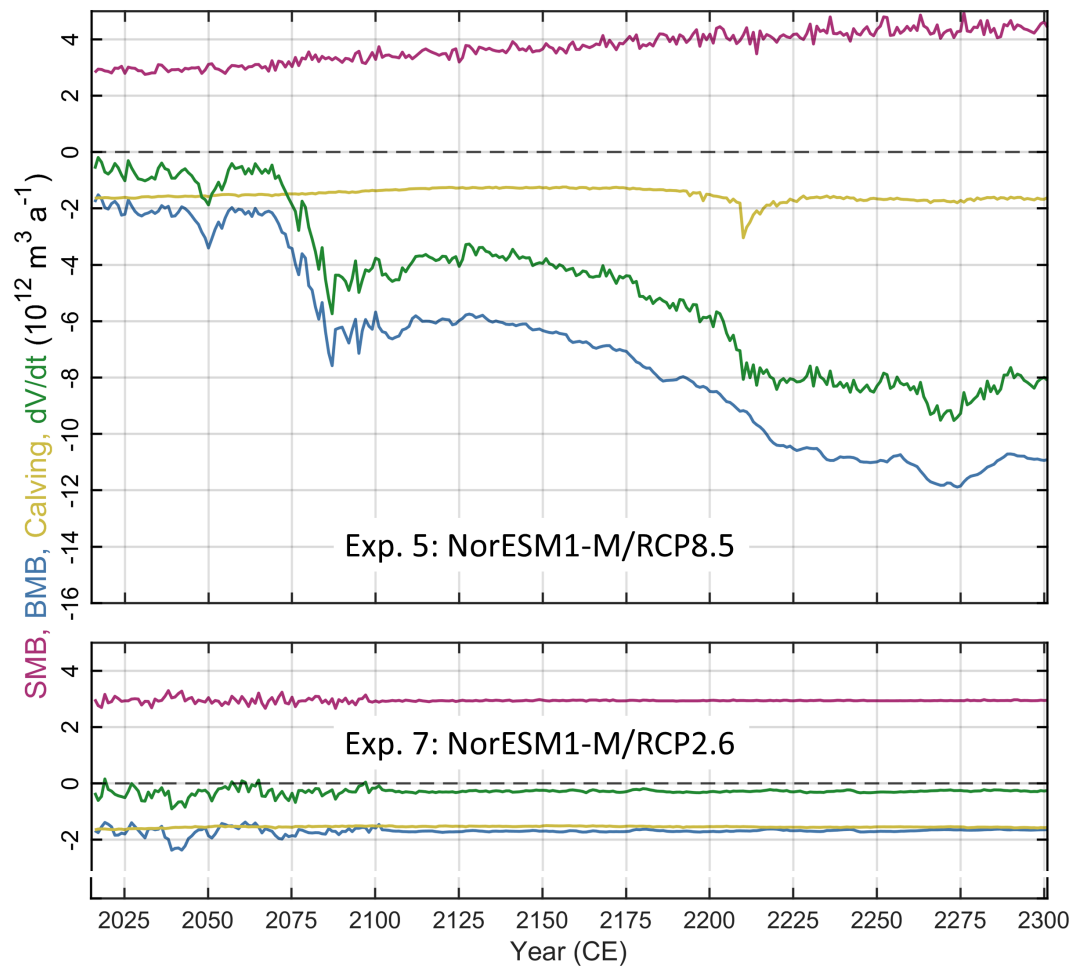


Fig. 6. Main components of the global mass balance for Exps. 5 and 7 (NorESM1-M/RCP8.5, NorESM1-M/RCP2.6): Surface mass balance (SMB, purple), basal mass balance (BMB, blue), calving (yellow) and ice volume change (dV/dt , green).